Article

Lessons Learnt from Modelling and Simulating the Bottom-Up Power System Restoration Processes

Roberto Benato , **Sebastian Dambone Sessa** and **Francesco Sanniti** *

Industrial Engineering Department, University of Padova, 35131 Padova, Italy; roberto.benato@unipd.it (R.B.); sebastian.dambonesessa@unipd.it (S.D.S.)
* Correspondence: francesco.sanniti@phd.unipd.it

Abstract: This paper aims to present the gained experience in modeling and simulating bottom-up power system restoration processes. In a system with low inertia, such as a restoration path, the Common Information Models for the regulation systems appear to no longer be suitable for the estimation of the frequency behavior, and thus a detailed model must be considered. On the other hand, due to the predominantly inductive behavior of the HV transmission network, the assumption of decoupling the power-frequency behavior to study the restoration stability seems to be licit. All these issues are discussed and justified in the paper by means of the use of different software packages and of the comparison with on-field recordings.

Keywords: power system restoration; primary frequency control; frequency nadir estimation; low inertia systems

1. Introduction

1.1. Motivations

In recent years, the studies on power system restoration are growing in importance since the massive replacement of the conventional generation set by converter-based resources is leading the bulk power system to be more sensitive to any transient contingency [1].

Therefore, the frequency deviations are becoming more and more prominent, and the eventuality of a system blackout is no longer a remote scenario. Besides the preventive and curative countermeasures, it is necessary to conceive strategies and restoration plans adapted to the new system paradigm: this ought to guarantee an electricity service recovery as quickly and safely as possible in case of wide outage. The modelling and simulation of the restoration plans, in addition to advanced transmission line modellings [2], make it possible to check, validate, and quickly modify the plan of the restoration processes.. From the authors' gained practice on modelling and simulation of bottom-up power system restoration processes, two questions arise:

- Is it licit to totally decouple the voltage and the frequency behavior for the dynamic simulation of a restoration process? How much does this assumption impact on the estimation of the frequency behaviour?
- Is it licit, as a first approximation, to simulate the restoration process by adopting the Common Information Models (CIMs) in the regulation sets? How much does this choice impact on the estimation of the frequency behaviour?

In order to answer these questions, this paper evaluates the impacts of these assumptions, by comparing the results of the implemented models with the recordings of a real restoration process.

1.2. Literature Review

Research on power system restoration have traditionally focused on system operation issues [3], for which the main objective is the optimal allocation of resources to

restore and to maximize the portion of recovered load and minimize the outage time [4,5]. This is generally formulated as a constrained optimization problem [6]. The dynamic stability analysis of the restoration process has been widely investigated in the most recent decades of the last century [7–10] and has also been studied through mock drills [11–13].

In the last years, the research on power system restoration dynamic stability is growing in relevance [14–19] since the frequency deviations are becoming more and more prominent, and so a correct estimation of transient behaviour is crucial.

In particular, in [14], a simple yet effective model for the simulation of restoration processes has been implemented by the authors. In that model, the decoupling between the voltage and frequency behaviours is the starting assumption. This assumption allows the authors to very significantly simplify the model by considering the restoration dynamic only based on the swing equation. In the present paper, a final validation of the model proposed in [14] is provided by comparing the decoupled model and the complete electromechanical model of a restoration path. Although this approximation is well-known in literature [20], this paper aims to quantitatively evaluate the impacts of this assumption by exploiting the recordings of a real restoration test.

With regard to the CIM modelling, the reference is the standard IEC 61970-302 [21], which is related to power systems dynamics: it currently has the primary use of facilitating the exchange of power system network data between organizations. In line with the ever-increasing standardization of power system devices, the authors think it is worth testing the dynamic performance of these models.

CIM models have already proven to be suitable for the estimation of the transient behaviour in highly interconnected power systems [22,23], but they do not provide any guarantee on their performance in low inertia systems, of which the restoration backbone is an example.

1.3. Contribution

The main contribution of this paper is summarized in Figure 1. The goal of this study is to quantitively evaluate the influence of different modelling approaches to represent the key elements involved in the restoration process by comparing the results of the simulations with the recordings of a real restoration process.
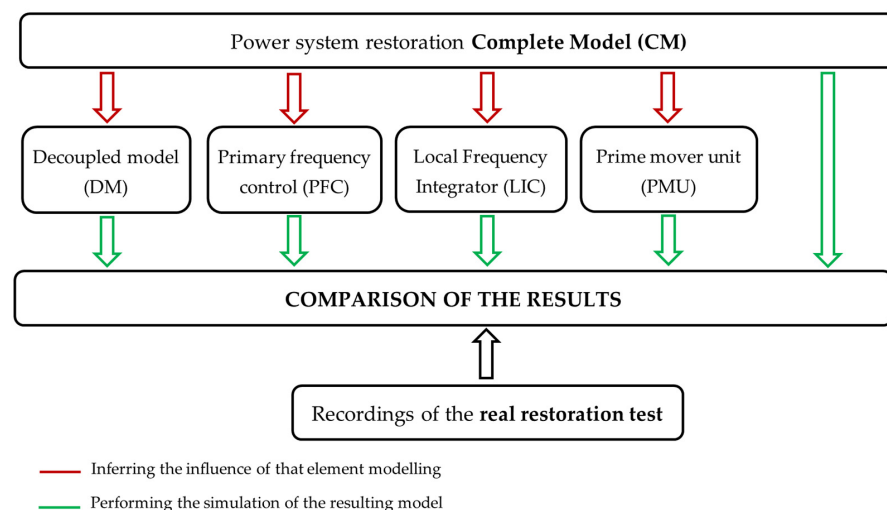
Figure 1. Visual scheme of the studies performed in this paper.

In Figure 1, the Complete Model (CM) must be intended as the detailed model of the real restoration path, including the actual configuration of the Primary Frequency Control (PFC), the Local Integrator Control (LIC), and the Prime Mover Unit (PMU) installed on the pilot generators. On the other hand, the Decoupled Model (DM) represents the same model but with the assumption of power-frequency decoupling. The red arrows indicates that an assumption is made on the CM. More specifically, the influence

of decoupling the frequency behaviour is studied as a first step. Then, the detailed models of PFC and the PMU are replaced one by one by their equivalent CIMs, leaving all the other elements of the CM unaltered. With regards to the LIC model, since there is no CIM equivalent model to represent it, its influence is studied by simulating the restoration with and without that element.

All the results are compared in terms of frequency deviations. The reason why the paper mainly focuses on frequency behavior is that this is the most critical dynamic in a bottom-up restoration process. In particular, it is important to be able to correctly estimate the frequency nadir, i.e., the minimum value the frequency reaches during the transient period. This index is important in a restoration framework since large frequency unbalances are expected after each load supply.

1.4. Organization

This paper is organized as follows. Section 2 describes the complete model of the restoration, the assumptions made for the decoupled model, and the simplified CIM models adopted for the purpose of comparison. Section 3 presents the results of the comparison between the measurement recording, the complete model, the decoupled model, and the adoption of the CIM models for the frequency regulation sets.

2. Power System Restoration Model

In this section, all the modelling features that influence the frequency behaviour during a restoration process are described. First, the focus is on the power system mathematical model and on assumptions needed to assume the decoupling between the frequency and the voltage behaviour. Thus, the models of the key elements that mostly affect the power-frequency behaviour are described: the PFC, the LIC, and PMU. In particular, PFC, LIC, and PMU are modelled by considering their actual set up, i.e., the real configuration of the regulators used during the real restoration is represented, without introducing simplifying hypotheses. Hence, the detailed models of PFC and PMU are compared with their equivalent CIM.

2.1. Power System Decoupling

With the aim of analyzing the rotor angle and the voltage stability of power systems, they are typically modelled by a set of non-linear Differential Algebraic Equations (DAEs), as follows:

$$\begin{aligned}\dot{x} &= f(x,y) \\ 0 &= g(x,y),\end{aligned} \tag{1}$$

where f and g are the differential and the algebraic equations, $x, x \in \mathbb{R}^n$ and $y, y \in \mathbb{R}^m$ are the state and algebraic variables, respectively. This model is widely adopted to represent the electromechanical behaviour of the system for transient stability analysis, i.e., for the time scale from 0.01 s to 10 s [20]. Now, let us consider a single source–a two-bus system with a lossless line and a load on bus 2, as depicted in Figure 2.

Assumed as a reference the phasor $v_2 \angle \vartheta_2$, such a system could represent the bulk power system of a bottom-up restoration. The lossless line is an acceptable assumption considering the low r/x ratio of the transmission lines. The set of equations in (1), if represented with the power-injection model [20], has two state equations:

$$\begin{aligned}\dot{\delta} &= \omega_n \Delta\omega \\ \dot{\omega} &= (p_m - p_e - D\Delta\omega)/T_a\end{aligned} \tag{2}$$

and two algebraic equations, related to the power-injections at bus (if one neglects the generator internal algebraic equations), as follows:

$$\begin{aligned}p_1 &= \frac{v_1 v_2}{x_L} \sin(\vartheta_1 - \vartheta_2) \\ q_1 &= \frac{v_1^2}{x_L} - \frac{v_1 v_2}{x_L} \cos(\vartheta_1 - \vartheta_2)\end{aligned} \tag{3}$$

where δ is the rotor angle, ω_n is the nominal angular speed in rad/s, $\Delta\omega_n$ is the angular speed deviation from the reference $\Delta\omega_{ref}$, p_m, and p_e are the mechanical and the electric power, respectively, D is the damping of the generator, T_a is the starting time of the generator ($T_a = 2H$ where H is the well-known inertia constant), p_1 and q_1 are the active and reactive power injected at bus 1, $v_1\angle\vartheta_1$ and $v_2\angle\vartheta_2$ are the voltage phasors at bus 1 and 2, respectively, and x_L is the line reactance.
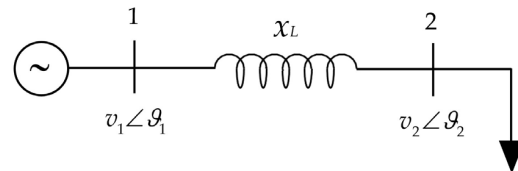

Figure 2. One machine, two-bus, one load system.

The differentiation of p_1 and q_1 in (3) leads to:

$$dp_1 = \frac{v_2}{x_L}\sin(\vartheta_1 - \vartheta_2)dv_1 + \frac{v_1 v_2}{x_L}\cos(\vartheta_1 - \vartheta_2)d\vartheta_1$$
$$dq_1 = \frac{2v_1 - v_2\cos(\vartheta_1 - \vartheta_2)}{x_L}dv_1 + \frac{v_1 v_2}{x_L}\sin(\vartheta_1 - \vartheta_2)d\vartheta_1. \tag{4}$$

Assuming as a first approximation that the angle deviation $\Delta\vartheta = \vartheta_1 - \vartheta_2$ is small, then $\sin\Delta\vartheta \approx \Delta\vartheta$ and $\cos\Delta\vartheta \approx 1$. Equation (4) yields:

$$dp_1 \approx \frac{v_1 v_2}{x_L}d\vartheta_1$$
$$dq_1 \approx \frac{2v_1 - v_2}{x_L}dv_1 \tag{5}$$

where the well-known concept that the angle deviation participates the most to the active power balance and the voltage deviations most affect the reactive power balance becomes clear. Therefore, since the commonly accepted definition of the frequency is the derivative of the voltage angle $\dot{\vartheta}$, the frequency of the system can be well-estimated by considering only the active power unbalances. In practice, this means that the model of the system is reduced to the second equation of (2), i.e., the swing equation of the system. The frequency, in the case of a single machine, is equivalent to the rotor angular velocity ω, and in the case of multiple machines, to the frequency of the Center of Inertia (COI) ω_{COI}, as:

$$\omega_{COI} = \frac{\sum_{i=1}^{N} T_{ai} S_i \omega_i}{\sum_{i=1}^{N} T_{ai} S_i} \tag{6}$$

where T_{ai}, S_i, ω_i are the starting time, the apparent power and the angular velocity of the i-th machine, respectively, and N is the number of machines involved in the restoration process.

Thus, the swing equation becomes:

$$\sum_{i=1}^{N} T_{ai}\dot{\omega}_{COI} = \sum_{i=1}^{N} p_{mi} - p_e - \sum_{i=1}^{N} D_i \Delta\omega_{COI} \tag{7}$$

where p_{mi} and D_i are the mechanical power and the damping coefficient of the i-th machine and p_e is the active power absorbed by the load, as the transmission lines are *transparent* for the active power flow. In the remainder of this paper, the notation CM indicates the implementation of the whole set of equations in (1), and DM indicates the implementation of (7). Note that p_{mi} in (7) is:

$$p_{mi} = (p_{PFCi} + p_{LICi}) \cdot p_{PMUi} \tag{8}$$

where p_{PFC} is the contribution of the PFC, p_{LIC} is the contribution of the LIC, and p_{PMU} involves the dynamic of the PMU. In the reminder of this section further details on the modelling of this contributions are given.

2.2. Primary Frequency Control

The detailed model of the primary frequency control is depicted in Figure 3.
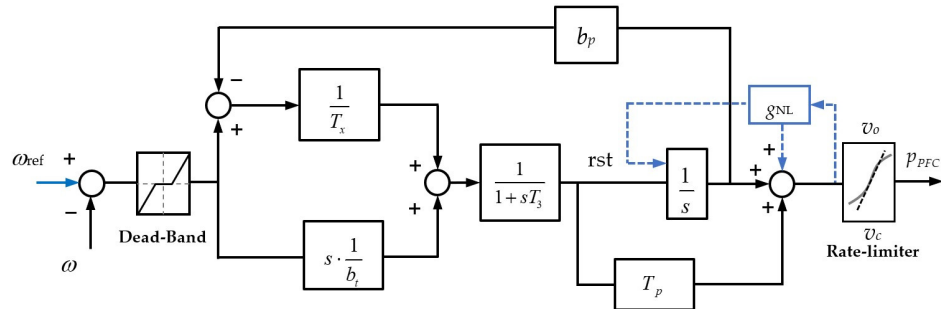

Figure 3. Control scheme of the detail model of the Hydro primary frequency regulation.

The model in Figure 3 represents the real regulation scheme implemented in the power plant object of the restoration path analysed in this paper.

Blue lines in Figure 3 refer to the control logic involved in the black-start phase during the dynamic transition from $\omega = 0$ to $\omega = \omega_n$. The starting phases of the generator start-up are the following:

- ω_{ref} is initialized to 0 and is then driven by a piece-wise ramp signal to reach the no-load speed value;
- when the generator reaches the no-load speed value, the actual value of p_{PFC} is memorized in the g_{NL} block and it is added to the total regulator output. At the same time, the integrator of the PFC is reset. This operation is required to memorize the value of the no-load gate opening of the turbine to avoid an unexpected response by the PFC during the normal operation;
- The generator parallel breaker is closed and the reference value ω_{ref} is set to its nominal value.

The equivalent transfer function of the PFC around the nominal speed is:

$$G_{PFC}(s) = \frac{1}{b_p} \frac{\left(1 + s\frac{T_x}{b_t}\right)\left(1 + sT_p\right)}{\left(1 + s\frac{T_x}{b_p}\right)\left(1 + sT_3\right)}. \tag{9}$$

The equivalent model of this regulator in the CIM library is the GovHydroIEEE2 (from now on called HG2) model [21] depicted in Figure 4. Note that all equivalent models found in literature do not involve the generator start up logics and instead only describe the model around its nominal speed.
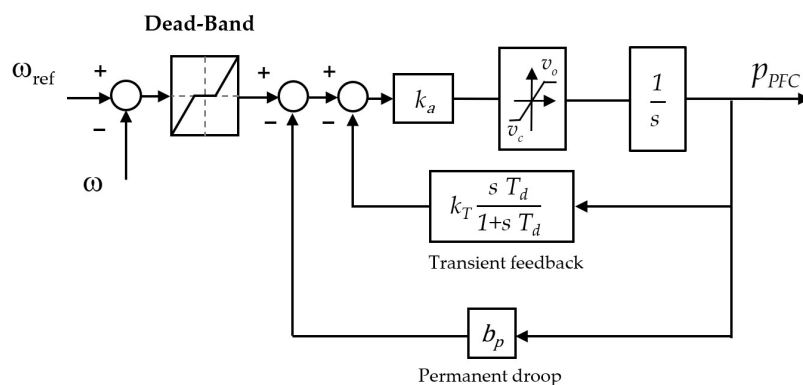

Figure 4. Control scheme of the HG2 model.

The conversion between the parameter set of the PFC and of the HG2 is as follows:

$$\begin{cases} T_d = T_x/b_p \\ k_T = b_t - b_p \end{cases} \tag{10}$$

2.3. Local Integration Control

The LIC is generally enabled for emergency condition frequency deviations and is always installed on the black start units. It ensures the perfect tracking of the frequency also for isolated generators without Automatic Generation Control (AGC) [24]. Compared to the AGC, however, the LIC is characterized by a higher gain to speed up the frequency restoration. The control scheme of the LIC is depicted in Figure 5.
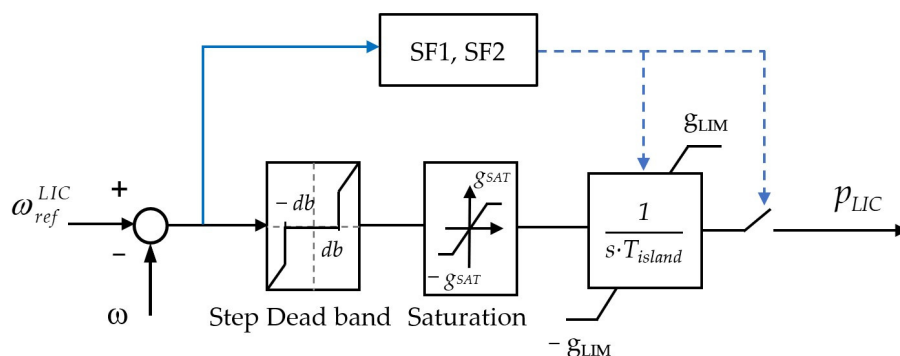

Figure 5. Control scheme of the LIC.

The logic function that controls the LIC action is highlighted by blue in Figure 5. The SF1 constant is the frequency threshold which determines the activation of the LIC control, whereas SF2 determines the condition for the disconnection of the LIC, i.e., when the system frequency stays beyond the SF2 threshold for at least T_{SF2} seconds. The disconnection action also resets the LIC integrator. The saturation block limits the frequency deviation to a maximum value g_{SAT} to avoid overshot behaviour in the LIC response in case of grid frequency peaks. As already mentioned, since there is no CIM representation for the LIC, no comparison is possible and so the LIC influence is studied in Section 3 by simulating the restoration with and without this element.

2.4. Prime Mover Model

The prime mover unit of the hydroelectric power plant considered in this study consists of a Francis turbine supplied by a forebay through a penstock pipe.

The adopted model involves the turbine model as well as the model of the hydro penstock. For the purpose of this study, the most detailed model of the penstock is adopted, i.e., the model that considers the elasticity of the penstock. Starting from the prime mover model of [25] (p. 416), the function $F(s)$ is derived as follows:

$$F(s) = \frac{dH}{dU} = -\left(\phi_p + Z_p \tanh(T_{ep}s)\right) \tag{11}$$

where dH is the deviation in the head of the water column, dU is the deviation on the water flow, ϕ_p is the penstock friction, Z_p is the equivalent penstock impedance, and T_{ep} is the penstock elastic time. Now, by replacing the hyperbolic tangent with its exponential series, it yields:

$$dH = dU \cdot Z_p \left(e^{-2T_{ep}s} - 1 - \phi_p\right) - dH \cdot e^{-2T_{ep}s} \tag{12}$$

This relation is implemented in the global prime mover model by exploiting the block algebra, as shown in Figure 6.
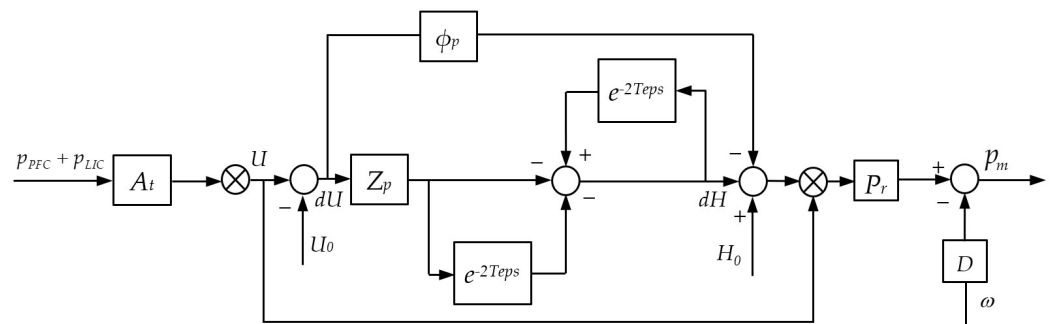
Figure 6. Detailed model of the prime mover.

With regards to the CIM equivalent representation of the PMU, there are many different equivalent representations in literature depending on the turbine type. Nevertheless, for the purpose of this study, the authors adopt the commonly accepted model of the prime mover for transient stability studies, which links the mechanical power to the gate opening through a transfer function with one zero and one pole, as follows [25]:

$$p_m = (p_{PFC} + p_{LIC}) \frac{1 - T_w s}{1 + 0.5 T_w s} \tag{13}$$

where T_w is the water starting time. The relationship between T_w and the quantities that describe the detailed model are represented by (14):

$$T_w = Z_p T_{ep} \tag{14}$$

3. Case Study

The results presented in this section are based on a real bottom-up power system restoration test performed in the Italian Transmission Grid in 2019. The recordings of the restoration test are compared to the simulation results of the models presented in the previous section. Moreover, an extensive comparison between the detailed models and the standard models is carried out, even by changing the parameter settings.
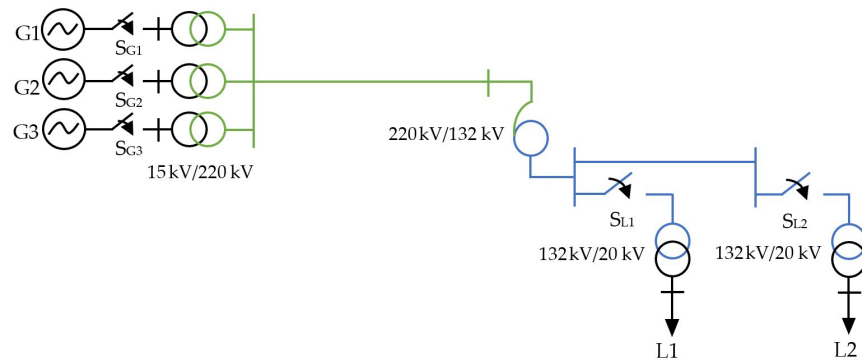
The restoration path is made up by:

- The pilot power plant, which is a hydroelectric power plant, where three parallel synchronous generators are installed;
- The target power plant, which is a thermoelectric power plant;
- Portions of the HV transmission grid;
- Portions of the distribution grid;

The restoration process starts with the black-start of the three hydro generators, then a portion of the HV transmission grid is supplied and at the same time some loads are restored by supplying the portions of the distribution grid. The final step is the parallel between the restoration path and the target power plant.

This work focuses on the study of the frequency behaviour during the start-up of the pilot generators and during the first two load restoration steps. A simplified scheme of the simulated restoration path is shown in Figure 7. In Figure 7, the black lines represent the medium voltage level (15 kV and 20 kV), the green lines represent the transmission voltage level (220 kV), and the blue lines represent the subtransmission voltage level (132 kV).

In Figure 7, G1, G2, G3 are the three hydro generators; L1 and L2 are the equivalent load representing a portion of a distribution grid; S_{G1}, S_{G2}, S_{G3}, S_{L1}, S_{L2} are the brakers that are closed during the restoration process to build the restoration path. With the aim of evaluating the performance of the model in terms of frequency deviations, the PQ power exchange of L1 and L2 is imposed externally by a measurement file taken from the measurement recordings.

Figure 7. Simplified single-line scheme of the restoration path.

The time domain simulations of the complete model are performed by the software package DIgSILENT PowerFactory; the simulations related to the decoupled model are instead performed in the Matlab-Simulink environment.

3.1. Measurements vs. Complete Model

Figure 8 shows the global results of the comparison between the real recording of the restoration test (Meas.) and the simulation results performed with the complete model. All the five switching closures of Figure 7 are simulated. The (a) graph of Figure 8 shows that the actual grid frequency is well-reproduced by CM, especially for the load step events S_{L1} and S_{L2}, which are the most critical operations for the restoration process. The (c) graph of Figure 8 shows the gate opening signal of G1. Even in this case, one can appreciate how the model correctly estimates the real behaviour. The (b) graph of Figure 8 is reported just for figuring the total active power absorbed by the restoration path. The simulated power is equivalent to the measured one, as expected, since the active flow is an input of the model, as discussed above.
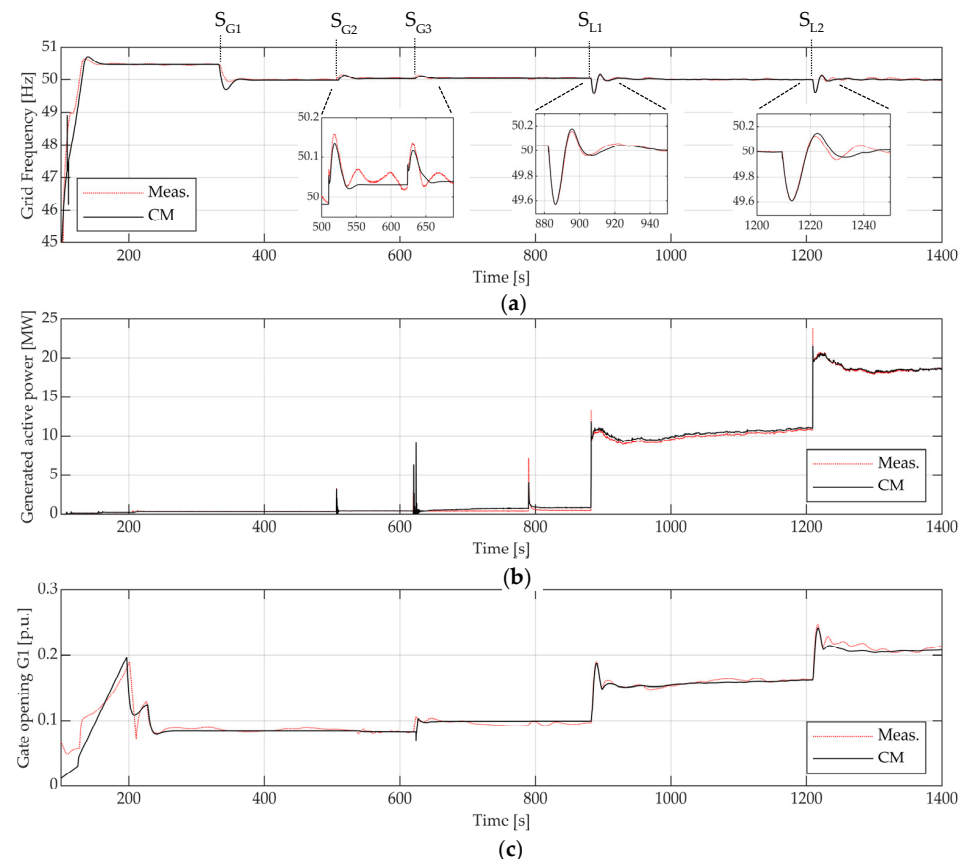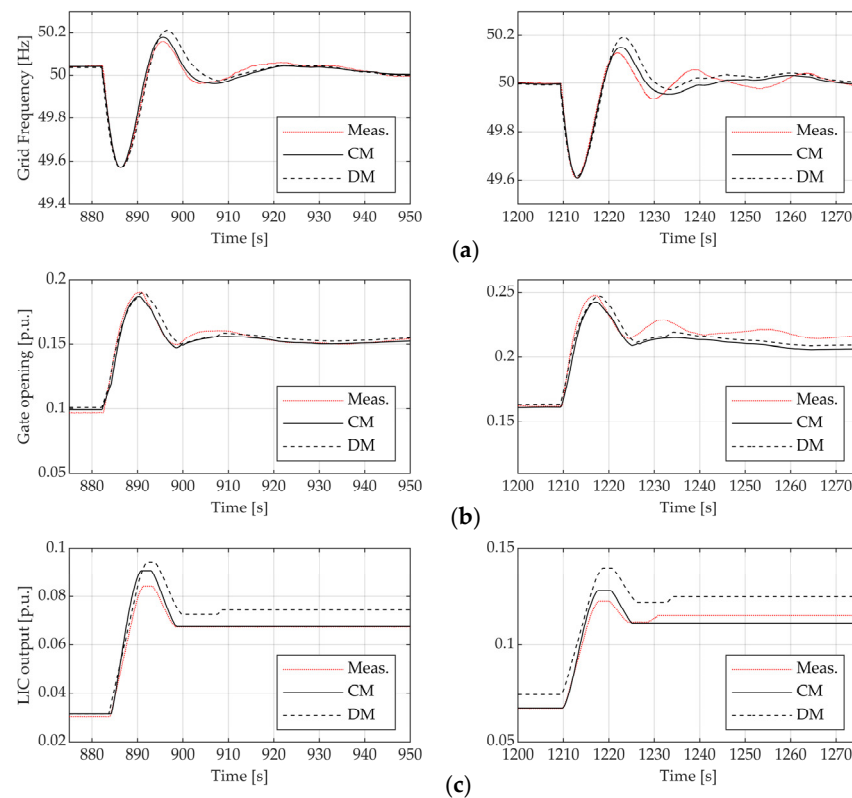

Figure 8. Comparison between simulation results and measurement recordings of the restoration test for (**a**) the grid frequency, (**b**) the generated active power and (**c**) the gate opening of G1.

3.2. Influence of the Power Frequency Decupling

In this section, the influence of the frequency–voltage decoupling assumption is discussed by comparing the simulation results of the decoupled model (DM) described in Section 2.1 with the results of the complete model (CM) and with the recording (Meas.). The focus, from now on, is on the results of the two load step events S_{L1} and S_{L2}, since they originate a transient response on which the models of interest have a higher influence. Figure 9 shows the transient behaviour of (a) the grid frequency, (b) the gate opening of the supply system of GRA, and (c) the output signal of the LIC of G1. The results show that the DM gives a perfect estimation of the frequency behaviour except for the frequency overshoot, for which the maximum error respect to the real behaviour is 0.04 Hz, see Figure 9c. This important result allows us to consider DM as a licit approximation of the CM to study the frequency behaviour during a restoration process. Nevertheless, in the remainder of this section, the simulations are performed by adopting the CM approach. This choice is made in order to separate the error (even if very small) introduced by adopting the DM from the influence of the single components modelling approach. In this way, it is possible to better allocate the cause of potential displacements in the simulation results.

Figure 9. Comparison between simulation results and measurement recordings of the S_{L1} and S_{L2} events for (**a**) the grid frequency, (**b**) the gate opening of G1, and (**c**) the output signal of the LIC of G1 for different mathematical models.

3.3. Primary Frequency Regulation Influence

In this section, the influence of different modelling of the PFC described in Section 2.2 is discussed. In particular, the complete model (CM) is compared with the HG2 model with the parameters derived from (10) (HG2), and the HG2 model with the standard parameters given in [21] (HG2 std.). The parameters of the PFC set in the three models are given in Table 1. The result of the comparison is depicted in Figure 10 for (a) the grid frequency and for (b) the gate opening of the supply system of G1.

Table 1. Parameters related to different models of the PFC.

Model	b_p [-]	b_t [-]	$T3$ [s]	T_p [s]	v_o [pu/s]	v_c [pu/s]	T_x [s]	T_d [s]	k_a [-]	k_t [-]
CM	0.04	0.4	0	0	0.07	0.15	2.3	-	-	-
HG2	0.04	0.4	-	-	0.07	0.15	2.3	5.75	100	0.36
HG2 std	0.05	0.55	-	-	0.1	0.1	6	12	2	0.5

The results show that the HG2 model returns a good estimation of the frequency behaviour, with a relative error on the frequency undershoot of 6.2% instead of the 25% given by the HG2 std. model. The quantitative behaviour of HG2 std. is also delayed with respect to the real behaviour for 4 s.

Figure 10. Comparison between simulation results and measurement recordings of the S_{L1} and S_{L2} events for (**a**) the grid frequency and (**b**) the gate opening of G1 for different model of the PFC.
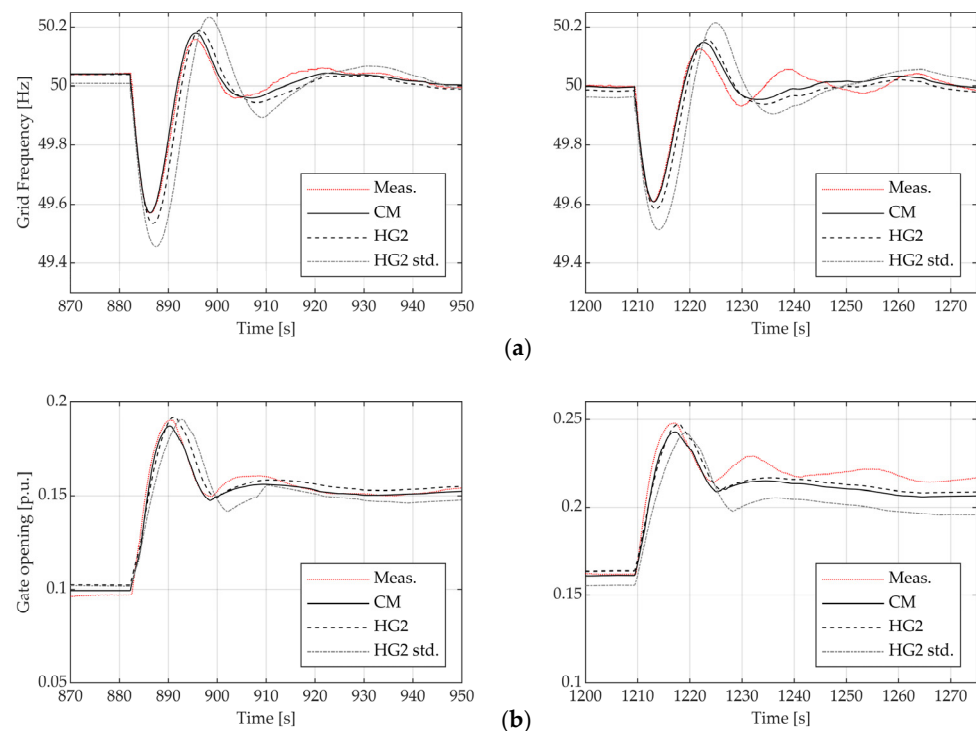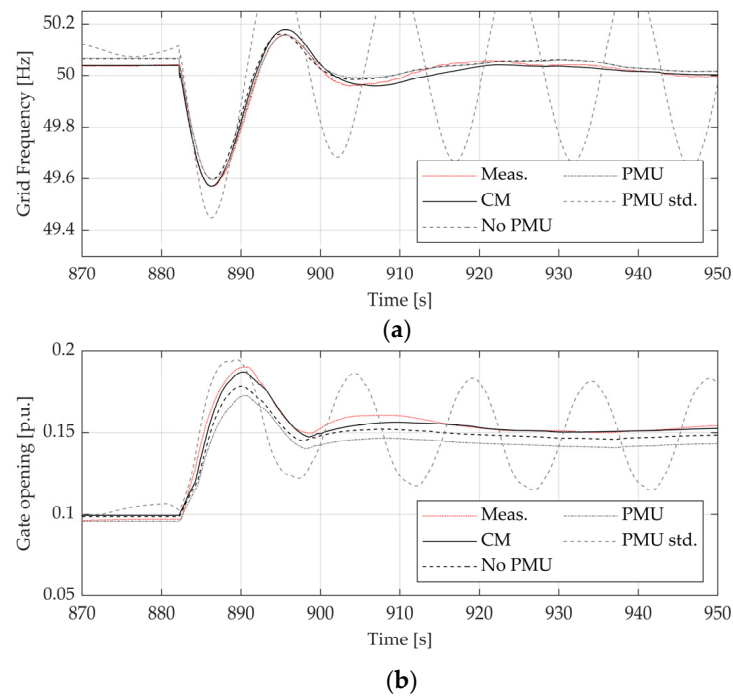
3.4. Prime Mover Unit Influence

In this section, the influence of the different modelling of the PMU described in Section 2.3 is discussed. In particular, the complete model (CM) is compared with the complete model without the prime mover model (No PMU), the complete model with the standard PMU model and with the parameters derived from (13) (PMU), and the complete model with the standard PMU model and the standard parameters given in [21] (PMU std.). The parameters of the PMU set in the three models are given in Table 2. The results of the comparison are depicted in Figure 11 for (a) the grid frequency and for (b) the gate opening of the supply system of G1.

Table 2. Parameters related to different models of the PMU.

Model	A_t [-]	Z_p [-]	ϕ_p [-]	T_{ep} [s]	D [pu]	P_r [pu]	T_w [s]
CM	1.12	1.52	0.001	0.23	0.08	0.77	-
PMU	-	0.4	-	0.23	-	-	0.35
PMU std	-	-	-	-	-	-	2

The results show how the model of the prime mover does not significantly affect the frequency behaviour, since the relative error of the frequency undershoot between Meas and No PMU is 6%. Moreover, the influence of using the standard prime mover model with the real parameters is extremely low; indeed, the curves of No PMU and PMU are overlapped. On the contrary, the standard prime mover model with the standard parameter leads to the rise of permanent wide oscillations in the frequency and in the gate opening behaviour, resulting in a completely wrong estimation of the real behaviour.

Figure 11. Comparison between simulation results and measurement recordings of the S_{L1} event for (**a**) the grid frequency and (**b**) the gate opening of G1 for different model of the PMU.

### 3.5. Local Integrator Control Influence

In this section, the influence of the presence of the LIC on the overall behaviour of a restoration process is discussed. In this case, the comparison with the equivalent standard model is not performed since there is no equivalent CIM model for the LIC.

In particular, the complete model (CM), which includes the LIC model, is compared with the complete model without the LIC (No LIC). The parameters of the LIC are given in Table 3. The results of the comparison are depicted in Figure 11 for (a) the grid frequency and for (b) the gate opening of the supply system of G1.

Table 3. Parameters of the LIC model.

Model	T_{island} [s]	$SF1$ [Hz]	$SF2$ [Hz]	db [Hz]	g_{SAT} [Hz]	g_{LIM} [pu]	T_{SF2} [s]
LIC	120	0.3	0.03	0.075	0.3	1	300

It is worth remembering that a standard AGC normally works in a higher time scale with respect to the PFC. On the contrary, the LIC action is faster, as it is possible to appreciate from Figure 12, since the presence of the LIC completely alters the PFC response and significantly contributes to the frequency restoration and to the nadir containment.
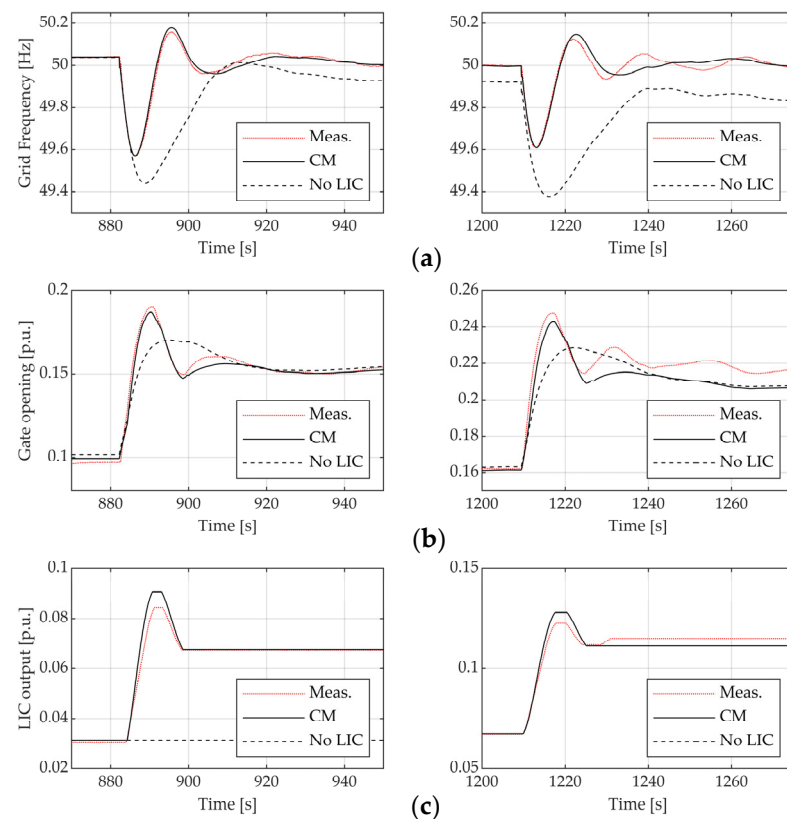
Figure 12. Comparison between simulation results and measurement recordings of the S_{L1} and S_{L2} events for (**a**) the grid frequency, (**b**) the gate opening of G1 and (**c**) the output signal of the LIC of G1, with and without the LIC model.

4. Conclusions

In this paper, a detailed model simulating a power system restoration process is presented and tested on a real restoration test. The proposed model correctly estimates the frequency behaviour during the load restoration and is proven to be effective, even for out-of-nominal conditions. (e.g., during the start-up of the generator).

Moreover, the results highlight how the assumption of the voltage-frequency decoupling does not significantly affect the frequency behaviour. This confirms the effectiveness of the simplified model presented in [13] as a powerful tool for the estimation of the frequency deviations during a restoration process. It could give the TSO useful decision support to determine the feasibility of a given restoration path.

The results of the comparison between the detailed model of the PFC and the PMU with their equivalent CIM models highlight, in some cases, a displacement on the estimation of the frequency Nadir. This happens when the CIM models are adopted by applying the IEC proposed parameters. Although the CIM models with standard parameters are more than suitable to estimate the transient behavior for a highly interconnected bulk power system, the paper demonstrates that, in the case of an islanded transmission system, the CIM models only work correctly if real parameters are adopted. In fact, for the analyzed case study, it was possible to combine the real parameters with the CIM structure. However, in general, it is very difficult to use real parameters by maintaining the IEC proposed CIM structure.

Hence, the knowledge of the actual regulation sets is of great relevance to correctly estimate the transient behaviors. In fact, a simplified representation of these components could lead to a wrong estimation of the frequency behaviour., e.g., when considering the standard parameters of the regulations sets.

Eventually, the results show how the influence of the LIC during a restoration process is prominent and how its action is overlapped with the action of the PFC, differently from what one might expect from an ACG in normal operation.

Author Contributions: Conceptualization, R.B. and F.S.; methodology, F.S. and S.D.S.; software, F.S.; validation, F.S.; formal analysis, F.S. and S.D.S.; investigation, F.S.; resources, F.S. and R.B.; data curation, F.S.; writing—original draft preparation, F.S.; writing—review and editing, F.S., R.B. and S.D.S.; visualization, S.D.S.; supervision, R.B.; project administration, R.B.; funding acquisition, F.S. All authors have read and agreed to the published version of the manuscript.

Conflicts of Interest: The authors declare no conflict of interest.

Acronyms

AGC	Automatic Generation Control
CIM	Common Information Model
CM	Complete Model
COI	Center Of Inertia
DAE	Differential Algebraic Equation
DM	Decoupled Model
HG2	GovHydroIEEE2
HV	High Voltage
LIC	Local Integrator Control
PFC	Primary Frequency Control
PMU	Prime Mover Unit
TSO	Transmission System Operator

References

1. Milano, F.; Dörfler, F.; Hug, G.; Hill, D.J.; Verbič, G. Foundations and Challenges of Low-Inertia Systems (Invited Paper). In Proceedings of the 2018 Power Systems Computation Conference (PSCC), Dublin, Ireland, 11–15 June 2018; pp. 1–25.
2. Benato, R.; Dambone Sessa, S.; Gardan, G.; Palone, F.; Sanniti, F. Experimental Harmonic Validation of 3D Multiconductor Cell Analysis: Measurements on the 100 km Long Sicily-Malta 220 kV Three-Core Armoured Cable. *IEEE Trans. Power Deliv.* **2022**, *37*, 573–581. [CrossRef]
3. Liu, Y.; Fan, R.; Terzija, V. Power System Restoration: A Literature Review From 2006 to 2016. *J. Mod. Power Syst. Clean Energy* **2016**, *4*, 332–341. [CrossRef]
4. Patsakis, G.; Rajan, D.; Aravena, I.; Rios, J.; Oren, S. Optimal Black Start Allocation for Power System Restoration. *IEEE Trans. Power Syst.* **2018**, *33*, 6766–6776. [CrossRef]
5. Liu, S.; Podmore, R.; Hou, Y. System Restoration Navigator: A Decision Support Tool for System Restoration. In Proceedings of the 2012 IEEE Power and Energy Society General Meeting, PES 2012, San Diego, CA, USA, 22–26 July 2012; IEEE Computer Society: San Diego, CA, USA, 2012.
6. Sun, W.; Liu, C.-C.; Zhang, L. Optimal Generator Start-up Strategy for Bulk Power System Restoration. *IEEE Trans. Power Syst.* **2011**, *26*, 1357–1366. [CrossRef]
7. Special Consideration in Power System Restoration. The Second Working Group Report. *IEEE Trans. Power Syst.* **1994**, *9*, 15–21. [CrossRef]
8. Adibi, M.M.; Borkoski, J.N.; Kafka, R.J.; Volkmann, T.L. Frequency Response of Prime Movers during Restoration. *IEEE Trans. Power Syst.* **1999**, *14*, 751–756. [CrossRef]
9. Adibi, M.M.; Borkoski, J.N.; Kafka, R.J. Analytical Tool Requirements for Power System Restoration. In *Power System Restoration: Methodologies and Implementation Strategies*; Wiley-IEEE Press: Hobocken, NJ, USA, 2000; pp. 86–95.
10. Delfino, B.; Invernizzi, M.; Morini, A. Knowledge-Based Restoration Guidelines. *IEEE Comput. Appl. Power* **1992**, *5*, 54–59. [CrossRef]
11. Mariani, E.; Mastroianni, F.; Romano, V. Field Experiences in Reenergization of Electrical Networks from Thermal and Hydro Units. In *Power System Restoration: Methodologies and Implementation Strategies*; Wiley-IEEE Press: Hobocken, NJ, USA, 2000; pp. 354–360.
12. Sforna, M.; Bertanza, V.C. Restoration Testing and Training in Italian ISO. *IEEE Trans. Power Syst.* **2002**, *17*, 1258–1264. [CrossRef]

13. Delfino, B.; Denegri, G.B.; Invernizzi, M.; Morini, A.; Cima Bonini, E.; Marconato, R.; Scarpellini, P. Black-Start and Restoration of a Part of the Italian HV Network: Modelling and Simulation of a Field Test. *IEEE Trans. Power Syst.* **1996**, *11*, 1371–1379. [CrossRef]

14. Benato, R.; Bruno, G.; Sessa, S.D.; Giannuzzi, G.M.; Ortolano, L.; Pedrazzoli, G.; Poli, M.; Sanniti, F.; Zaottini, R. A Novel Modeling for Assessing Frequency Behavior During a Hydro-to-Thermal Plant Black Start Restoration Test. *IEEE Access* **2019**, *7*, 47317–47328. [CrossRef]

15. Benato, R.; Giannuzzi, G.M.; Poli, M.; Sanniti, F.; Zaottini, R. A Fully Decoupled Model for the Study of Power-Frequency Behaviour during a Power System Restoration Test. In Proceedings of the 2020 AEIT International Annual Conference (AEIT), Bari, Italy, 23–25 September 2020; pp. 1–6.

16. Benato, R.; Giannuzzi, G.M.; Masiero, S.; Pisani, C.; Poli, M.; Sanniti, F.; Talomo, S.; Zaottini, R. Analysis of Low Frequency Oscillations Observed During a Power System Restoration Test. In Proceedings of the 2021 AEIT International Annual Conference (AEIT), Milan, Italy, 4–8 October 2021; pp. 1–6.

17. Benato, R.; Giannuzzi, G.M.; Poli, M.; Sanniti, F.; Zaottini, R. The Italian Procedural Approach for Assessing Frequency and Voltage Behavior during a Bottom-up Restoration Strategy. In Proceedings of the 2020 IEEE International Conference on Environment and Electrical Engineering and 2020 IEEE Industrial and Commercial Power Systems Europe (EEEIC/I CPS Europe), Madrid, Spain, 9–12 June 2020; pp. 1–6.

18. Benato, R.; Bruno, G.; Pedrazzoli, G.; Giannuzzi, G.M.; Ortolano, L.; Zaottini, R.; Poli, M.; Sanniti, F. An Experimental Validation of Frequency Model for Studying a Real Black Start Restoration. In Proceedings of the 2019 AEIT International Annual Conference (AEIT), Florence, Italy, 18 September 2019; pp. 1–6.

19. Hachmann, C.; Lammert, G.; Lafferte, D.; Braun, M. Power System Restoration and Operation of Island Grids with Frequency Dependent Active Power Control of Distributed Generation. In Proceedings of the 5th Conference on Sustainable Energy Supply and Energy Storage Systems, NEIS 2017, Hamburg, Germany, 21–22 September 2017; pp. 45–50.

20. Milano, F. *Power System Modelling and Scripting*, 2010 ed.; Springer: Berlin/Heidelberg, Germany, 2010.

21. *IEC 61970-302*; Common Information Model (CIM) Dynamics, Version 1. IEC: Geneva, Switzerland, 2018.

22. Gomez, F.J.; Vanfretti, L.; Olsen, S.H. CIM-Compliant Power System Dynamic Model-to-Model Transformation and Modelica Simulation. *IEEE Trans. Ind. Inform.* **2018**, *14*, 3989–3996. [CrossRef]

23. Semerow, A.; Hohn, S.; Luther, M.; Sattinger, W.; Abildgaard, H.; Garcia, A.D.; Giannuzzi, G. Dynamic Study Model for the Interconnected Power System of Continental Europe in Different Simulation Tools. In Proceedings of the IEEE Eindhoven PowerTech, PowerTech 2015, Eindhoven, The Netherlands, 29 June–2 July 2015; Institute of Electrical and Electronics Engineers Inc.: Eindhoven, The Netherlands, 2015.

24. Ross, H.B.; Giri, J.; Kindel, B. An AGC Implementation for System Islanding and Restoration Conditions. In *Power System Restoration: Methodologies and Implementation Strategies*; Wiley-IEEE Press: Hobocken, NJ, USA, 2000; pp. 75–85.

25. Kundur, P. *Power System Stability and Control*; McGraw Hill: New Delhi, India, 2008.